https://doi.org/10.5194/os-2021-38
Preprint. Discussion started: 25 May 2021

Ocean Science
Discussions

Geophysical and biogeochemical observations using BGC Argo floats in the western North Pacific during late winter and early spring. Part 1: Restratification processes of the surface mixed layer

Ryuichiro Inoue[1], Chiho Sukigara[2], Stuart Bishop[3], Eitarou Oka[4], Takeyoshi Nagai[2]

Correspondence to: Ryuichiro Inoue (rinoue@jamstec.go.jp)

[1] Japan Agency for Marine-Earth Science and Technology, Yokosuka, Kanagawa 237-0061, Japan.

[2] Tokyo University of Marine Science and Technology, Minato, Tokyo, 108-8477, Japan

[3] North Carolina State University, Raleigh, North Carolina, 27695, USA

[4] University of Tokyo, Kashiwa, Chiba, 277-0882, Japan

https://doi.org/10.5194/os-2021-38
Preprint. Discussion started: 25 May 2021

Abstract. To understand oceanic restratification in the subtropical northwestern Pacific and its influence on biogeochemical (BGC) processes, we examined post-storm restratification events observed from February to April 2018 by BGC-Argo floats, the BGC data from which were stoichiometrically analyzed by Sukigara et al. (2021; this issue). We found that during these events, restratification of the mixed layer (ML) was driven by geostrophic adjustment or ML eddy formation related to surface cooling during February to March. At the end of March, high surface chlorophyll *a* concentrations were observed within submesoscale eddies and at the edge of a mesoscale cyclonic feature observed from satellite data. Our results indicate that primary production in the subtropical northwestern Pacific is enhanced by the combined effects of mesoscale upwelling, storm-driven formation of a deep ML, subsequent formation of ML eddies, weak cooling, and the length of intervals between storms.

https://doi.org/10.5194/os-2021-38
Preprint. Discussion started: 25 May 2021

Ocean Science Discussions

1. Introduction

In the subtropical northwestern Pacific Ocean, the effects of large wintertime air–sea buoyancy fluxes and wind forcing result in formation of a deep mixed layer (ML). The mixed water is eventually subducted into the ocean interior to become North Pacific Subtropical mode water (NPSTMW), which is an important storage reservoir for anthropogenic carbon (e.g. Oka et al., 2018 and 2019). The northwestern Pacific Ocean also plays an important role in carbon fixation through net community production (e.g., Riser and Johnson, 2008). Fassbender et al. (2017) used data from the Kuroshio Extension observatory buoy site (Cronin et al., 2013) in the region where the NPSTMW forms to quantitatively estimate the export of organic and inorganic carbon from the surface to the ocean interior. They demonstrated that the amount of nutrients available for phytoplankton is controlled by the balance between the maximum ML depth in winter, the speed of shallowing of the ML in spring, and light conditions in the euphotic zone.

The shallowing of the ML in spring is caused by surface warming due to solar radiation and one-dimensional air–sea heat exchange, although Mahadevan et al. (2012) showed that rapid restratification in ocean frontal regions is related to the formation of ML eddies, whose strength depends on mesoscale horizontal density gradients. Fox-Kemper et al. (2008) showed that horizontal density differences within the ML generates ML eddies that work to rapidly restratify surface waters. However, it takes more than several days for the ML to reach baroclinic

https://doi.org/10.5194/os-2021-38
Preprint. Discussion started: 25 May 2021

instability, so it is possible that the initial geostrophic adjustment is important (Tandon and Garrett, 1995) if the intervals between storms are shorter than the time scale of baroclinic instability. Tandon and Garrett (1995) also pointed out that symmetric instability (e.g., Stone, 1970) might be important during the initial geostrophic adjustment, which has also been demonstrated by numerical simulations (Taylor and Ferrari, 2009). Furthermore, weakly stratified waters near eddy edges create density fronts, which can enhance vertical mixing through slantwise convection caused by symmetric instability forced by down-front winds and submesoscale (~10 km) cooling (Taylor and Ferrari, 2010).

Because it is difficult to obtain data of high temporal and spatial resolution in the northwestern Pacific during severe winter weather, the abovementioned stratification and de-stratification processes have rarely been observed, so their effects on biogeochemical (BGC) cycling are not well understood (Mahadevan, 2016).

To better understand the influence of submesoscale physical processes on BGC processes in the subtropical northwestern Pacific, we conducted BGC and microstructure turbulence measurements during two cruises in January and April 2018. To fill the observational gap between the two cruises, we deployed two BGC floats (NAVIS, Sea-Bird Scientific, Bellevue, USA), one Electro-magnetic-APEX float (Teledyne Webb Research, MA, USA), and one SeaGlider (Kongsberg Maritime, Kongsberg, Norway) during the first cruise (on 28 January

https://doi.org/10.5194/os-2021-38
Preprint. Discussion started: 25 May 2021

2018) and compared the data acquired with them with high-resolution satellite data. Our aim was to use these data to clarify the physical oceanographic conditions during post-storm restratification events in the subtropical northwestern Pacific.

2. Data and methods

2.1. Biogeochemical floats

On 28 January 2018, during R/V *Shinsei Maru* cruise KS-18-1 (January 18-30, 2018), two NAVIS BGC floats (World Meteorological Organization nos. 2903329 and 2903330) were launched at 33.25°N, 142.50°E in the Kuroshio recirculation gyre, south of the Kuroshio Extension (Fig. 1; see also Sukigara et al. (2021; this issue). Until 13 March, the floats moved southwestward separated by <20 km. They then turned northward in the region between the –4000 and –3000 m isobaths, maintaining a separation thereafter of about 25 km. On 10 April they reached the Kuroshio Extension and were swept northeastward until April 20, 2018 when those were recovered in R/V *Shinsei Maru* cruise KS-18-4 (April 20-May 1, 2018).

Each float was equipped with an SBE41CP conductivity–temperature–depth (CTD) sensor (Sea-Bird Electronics, Inc., Bellevue, USA) and BGC sensors. In this study, we used the CTD data from the floats; the BGC data have been discussed by Sukigara et al. (2021; this issue).

https://doi.org/10.5194/os-2021-38
Preprint. Discussion started: 25 May 2021

After descending from a parking depth of 1000 dbar to a depth of 2000 dbar, the floats measured CTD data (vertical sampling interval of 2 dbar) during their subsequent ascent to the sea surface. Each float reached the sea surface at about midnight and remained there for about 15 min to transmit data via the IRIDIUM satellite-based wireless communication system before returning to the parking depth. The same procedure was repeated daily during the two cruises.

2.2. Other data sets

We used daily mean global eddy-resolving ocean reanalysis data (1/12° horizontal resolution, Global_ReAnalysis_phy_001_030; provided by the Copernicus Marine Environment Monitoring Service; http://marine.copernicus.eu) covering the float observation period.

We used 1/4° × 1/4° daily gridded sea surface height anomaly (SSHA) from the Archiving, Validation, and Interpretation of Satellite Oceanographic (AVISO) dataset (Ducet et al., 2000) and chlorophyll-a from Moderate Resolution Imaging Spectroradiometer-Aqua (MODIS) satellite data. level 2 LAC (Local Area Coverage) data (https://oceancolor.gsfc.nasa.gov/cgi/browse.pl) on 15 March (A2018074031000.L2_LAC_OC.nc), 25 March (A2018084034500.L2_LAC_OC.nc) and 29 March (A2018088032000.L2_LAC_OC.nc).

We also used the ERA5 hourly reanalysis data from the European Centre for Medium-Range

https://doi.org/10.5194/os-2021-38
Preprint. Discussion started: 25 May 2021

Weather Forecasts (https://www.ecmwf.int/en/forecasts/datasets/reanalysis-datasets/era5) for surface heat fluxes and wind stresses during the observation period.

2.3. Heat budget of the upper ocean

Sukigara et al. (2021) showed that the atomic carbon to nitrogen (CN) ratios during four storm events observed by the BGC floats differed considerably (Table 1). Although the CN ratio immediately after a storm event does not necessarily correspond to the Redfield ratio (Redfield 1958), during two of those storms, the observed CN ratios did not match the Redfield ratio at all. The goal of the research we present here was to determine whether those differences of CN ratio were caused by physical oceanographic conditions. We therefore calculated the temporal changes of heat content and examined the one-dimensional heat budget of the upper ocean. If this heat balance does not hold, we speculate that other factors such as float movements and horizontal advection might be important.

Because the ML south of the Kuroshio Extension reaches a depth of 300 dbar, and to avoid estimating entrainment heat fluxes associated with its deepening, for both float profiles we calculated the heat content between the shallowest observed depth and 400 dbar. By assuming a negligibly small vertical heat flux across 400 dbar, the daily heat content change should be equal to the heat flux at the sea surface, expressed as

https://doi.org/10.5194/os-2021-38
Preprint. Discussion started: 25 May 2021

Ocean Science Discussions
Open Access

$$\rho C_p \Delta \int_{-400}^{0} \theta \, dz \sim \int_{0}^{1day} F_t|_{z=0} \, dt. \qquad (1)$$

Here, Δ is the difference between the two daily profiles and $F_t|_{z=0}$ is the surface heat flux.

We considered three types of surface heat flux: the air–sea heat flux and heat fluxes due to Ekman transport and ML eddy formation.

To consider the air–sea heat flux we interpolated hourly float positions between daily positions and then interpolated the ERA5 hourly reanalysis data to those positions. The interpolated hourly heat fluxes were integrated over 24 h and compared with the daily change of heat content.

To compare the daily heat content change with the heat flux due to Ekman transport (F_{EK}, Thomas and Lee, 2005) we used the following equation:

$$F_{EK} = -\frac{(\boldsymbol{\tau}\times\hat{k})\cdot\nabla_h b}{\rho_0 f}\frac{C_P \rho_0}{\alpha g} = -\frac{\tau_y \partial b/\partial x - \tau_x \partial b/\partial y}{f}\frac{C_P}{\alpha g}, \qquad (2)$$

where $\boldsymbol{\tau} = (\tau_x, \tau_y)$ is wind stress from the interpolated ERA 5 hourly reanalysis data, $\hat{k}$ is a unit vector, f is the Coriolis frequency, C_P is the specific heat of sea water, α is the thermal expansion coefficient of sea water, g is gravitational acceleration, and $\nabla_h b$ is the horizontal gradient of buoyancy. Here, we used the reanalysis data provided by the Copernicus Marine Environment Monitoring Service to estimate $\nabla_h b$ at the sea surface by center differentiation on each model grid and interpolated it to float positions at their surfacing times. Note that the reanalysis data cannot resolve the submesoscale differences related to the spatial separation of

https://doi.org/10.5194/os-2021-38
Preprint. Discussion started: 25 May 2021

the two floats. We also used the differences of the ML densities obtained by the two floats to calculate $\nabla_h b$ and compared the resultant values with the reanalysis data. In this approach, we used the wind stress normal to the line drawn between two floats' positions to calculate F_{EK}.

The heat flux due to ML eddy formation (F_{ME}, Fox-Kemper et al., 2008) is

$$F_{ME} = 0.06 \frac{|\nabla_h b|^2 H^2}{f} \frac{C_P \rho_0}{\alpha g} > 0, \tag{3}$$

where H is the average of the ML depths obtained from the two floats. ML depth was defined as the depth at which the potential density became 0.03 kg m^{-3} heavier than the average potential density above 10 dbar.

Note that the F_{EK} and F_{ME} values we determined represent upper bounds, because the time scale of those processes is longer than that of the initial geostrophic adjustments (less than a few days) (e.g., Thomas and Ferrari, 2008; Fox-Kemper et al., 2008).

3. Results

3.1. Atmospheric conditions during the period of the two BGC floats observations

In early February, a week or so of strong winds was followed by a few calm days. From the middle of February, the calm intervals between periods of strong wind were mostly longer than a few days (Fig. 2a). Hourly net sea-surface heat fluxes showed diurnal cycles (24-h averages

https://doi.org/10.5194/os-2021-38
Preprint. Discussion started: 25 May 2021

approaching zero), and cooling during storm events weakened approaching April (Fig. 2b). Sukigara et al. (2021; this issue) discuss the stoichiometry during restratification events following four storms (Table 1 and Fig. 2), which are also the focus of this study.

3.2. Float observations

The two BGC floats deployed in the Kuroshio recirculation gyre on 28 January 2018 indicated that the ML was deep (Fig. 3) during the period when the floats initially circled and began to move westward (Fig. 1). Isothermal heaving was apparent below the ML at various times. We examined the physical oceanographic conditions during a period of heaving between 11 and 18 March, which corresponds to the period of the third post-storm restratification event (Case 3 in Table 1). The deepest ML was observed between 18 and 25 March (which corresponds to Case 4). In April, the ML rose to a shallower level in response to atmospheric conditions and the positions of the two floats which approached to the Kuroshio Extension.

3.3. Changes of heat content

https://doi.org/10.5194/os-2021-38
Preprint. Discussion started: 25 May 2021

In this section, we focus on the four storm events recognized by Sukigara et al. (2021; this issue), all of which occurred between January and March (Table 1). The average temperature of the water column from the surface to the 400 dbar level (Fig. 4a) increased until 10 March, decreased suddenly around 11 March, and then started to increase again. Because surface heat fluxes measured in February and March showed cooling of the ocean surface, we suggest that the observed increases were likely caused either by lateral advection of warm water, or by lateral movement of the floats.

The largest values of F_{EK} and F_{ME} were of the same magnitude as the surface heat fluxes, except on 22 February (Fig. 4b). Comparison of the values of $\nabla_h b$ from the ocean reanalysis data with those determined from the float observations showed that F_{EK} from the reanalysis data tended to be larger. In contrast, the F_{ME} values determined from the float observations were larger than those from the reanalysis data. These differences indicate that $\nabla_h b$ may be underestimated in the reanalysis data, possibly because of differences in the horizontal resolution of the reanalysis data and float observations, and that the inner product of wind stress and $\nabla_h b$ estimated from float observations in (2) is also underestimated because winds normal to the line drawn between two floats' positions do not match the largest Ekman transport. The daily change of heat content is 10 times (or even more) the time-integrated net heat flux, which supports the importance of changes due to horizontal temperature gradients, even though there

https://doi.org/10.5194/os-2021-38
Preprint. Discussion started: 25 May 2021

Ocean Science Discussions Open Access EGU

are large uncertainties in estimating F_{EK} and F_{ME}. Our results suggest that of the post-storm events identified, only Case 4 is close to a one-dimensional exchange of heat budget in the upper 400 dbar of the water column.

Next, we examine the details of each of the post-storm restratification events shown in Table 1.

3.3.1. Case 1 (6–9 February, after the storm of 5 February)

After deployment on 28 January, the circling BGC floats drifted westward (Fig. 5a). After the storm on 5 February, deepening and cooling of the ML continued until 7 February (Fig. 5b-c); then, during 8–11 February, it shoaled and warmed. During 8–11 February, a warm front within the ML was identified near the western end of a SeaGlider transect across the float trajectory (Figs. 5a and 6). We therefore concluded that the warmer water encountered by the floats as they drifted westward after deployment represented a different water mass, which was substantiated by the low CN ratio of water sampled after the storm (Table 1).

3.3.2. Case 2 (18–23 February, after the storm of 17 February)

https://doi.org/10.5194/os-2021-38
Preprint. Discussion started: 25 May 2021

Ocean Science Discussions
Open Access

By 18 February the circling floats had drifted eastward and returned to the vicinity of their deployment (Fig. 7a), where the observed water temperature was lower compared to that in the west. The potential temperature in the ML above the 200 dbar level changed little but showed some evidence of restratification (Fig. 7b-c). Changes of heat content were mainly below the 200 dbar level; we therefore consider that below the 200 dbar level the floats were within the same water mass of the ML, which may explain why the estimated CN ratio (Table 1) was relatively close to the Redfield ratio. The restratification process within the ML is further discussed in the section 4.2.

3.3.3. Case 3 (9–15 March, after the storm of 7 March)

While the floats moved westward roughly along the sea surface height anomaly (SSHA) contour during this period (Fig. 8a), a cyclonic feature moved northward through the area and the floats observed a doming isotherm (Fig. 3) below the ML (Fig. 8c). The doming isotherm was accompanied by salinity intrusions (Fig. 8b), which disappeared when the floats left the doming structure. This mesoscale doming and the accompanying salinity intrusions are indicative of the importance of lateral processes, which may explain the large difference between the two CN ratios estimated during this period (Table 1).

https://doi.org/10.5194/os-2021-38
Preprint. Discussion started: 25 May 2021

3.3.4. Case 4 (22–27/28 March, after the storm of 21 March)

The floats moved northward during 22–27/28 March and the cyclonic structure retreated (Fig. 9a–b). We observed the deepest ML (~320 dbar) during this period, and potential temperature in the water column above it was relatively uniform and was gradually stratified during this period (Fig. 9c–d). Case 4 showed the largest increments of particulate organic carbon (POC) among the four events (Table 1). The increased POC might be explained by post-storm formation of submesoscale cyclonic eddies in the ML (Fig. 10), which trapped nutrients and phytoplankton near the surface during the calmer and warmer weather at the end of March (as discussed in section 3.1). Note that March 28 was chosen as the end of Case 4 for the float no. 2903330, which corresponded to the maximum concentration of chlorophyll *a* after the storm (Sukigara et al., 2021), and we speculate that the difference of dates is related to the patchiness of high chlorophyll *a* distribution seen in Figure 10c.

In the next section, we further explore the effects of mesoscale features during Cases 3 and 4 that could have enhanced submesoscale activities and the vertical transport of nutrients below the ML.

https://doi.org/10.5194/os-2021-38
Preprint. Discussion started: 25 May 2021

Ocean Science Discussions

4. Discussion

4.1. Effects of mesoscale features

It is known that moving cyclonic eddies promote local upwelling (McGillicuddy et al., 1998). In winter, enhanced entrainment of nitrate during deepening of the ML can be expected if there is a cyclonic eddy below the deep ML. To investigate vertical motion due to such mesoscale phenomena, we calculated the Q vector normalized by the horizontal buoyancy gradient $Q \cdot \nabla_h b / |\nabla_h b|$ and its negative horizontal divergence $-\nabla_h \cdot Q(\sim w)$.

If we assume a quasi-geostrophic balance, $Q \cdot \nabla_h b / |\nabla_h b|$ and $-\nabla_h \cdot Q(\sim w)$ correspond to changes of the horizontal gradient of buoyancy with time and vertical velocity, respectively. The $\boldsymbol{Q}$ vector (e.g. Hoskins et al., 1978) is defined as

$$\boldsymbol{Q} = (Q_1, Q_2) = \left(-\frac{\partial u}{\partial x}\frac{\partial b}{\partial x} - \frac{\partial v}{\partial x}\frac{\partial b}{\partial y}, -\frac{\partial u}{\partial y}\frac{\partial b}{\partial x} - \frac{\partial v}{\partial y}\frac{\partial b}{\partial y}\right). \quad (4)$$

We calculated the above variables at 400 m depth by using ocean reanalysis data (described in Section 2.2) that do not provide vertical velocity fields. We examined those variables in March, when both cyclonic features and high surface concentrations of chlorophyll *a* (e.g., Fig. 10c) were observed (during Cases 3 and 4).

https://doi.org/10.5194/os-2021-38
Preprint. Discussion started: 25 May 2021

The ***Q*** vector at 380 m depth (below the ML) indicated that the density field there was squeezed in early March when upwelling was observed at the edge of cyclonic features (Fig. 11a and d). From the middle of March, the density field became relaxed and the distribution of upwelling became patchy (Fig. 11b and e). By 21 March, the mesoscale changes of the density field and upwelling had slowed (Fig. 11c and f). We speculate that the patchy upwelling associated with mesoscale fluctuations of the density field in early and middle March increased local nutrient concentrations below the ML. Then, during sporadic storms toward the end of March, nutrients were entrained in the deepening ML and restratification due to ML eddies created high surface concentrations of chlorophyll *a* .

In the next section, we discuss restratification processes during Cases 2 and 4, when the heat budget indicated that the effects of horizontal advection and float movement on heat contents were small.

4.2. Potential vorticity budget

Based on the potential vorticity (PV) budget, the rate of change of stratification in the ML can be scaled by ML eddy formation, surface Ekman buoyancy flux, surface buoyancy flux, and geostrophic adjustment according to the relationships

https://doi.org/10.5194/os-2021-38
Preprint. Discussion started: 25 May 2021

$$\frac{\partial N_{ME}^2}{\partial t} \sim 0.06\,(\nabla_h b)^2/f,\ \frac{\partial N_{EK}^2}{\partial t} \sim -\frac{(\tau \times \hat{k}) \cdot \nabla_h b}{\rho_0 f H^2},\ \frac{\partial N_{BUO}^2}{\partial t} \sim -\frac{B_0}{H^2},\ \text{and}$$

$$\frac{\partial N_{GEO}^2}{\partial t} \sim (2\pi)^{-1}\,(\nabla_h b)^2/f, \qquad (5)$$

respectively (e.g., Tandon and Garrett, 1995; Wenegrat et al., 2018). Here, B_0 is surface buoyancy flux, which is approximated as $B_0 \approx -\alpha g F_T / C_p \rho_0$ (positive for cooling). For $\partial N_{GEO}^2/\partial t$, the inertial period was used as the time scale. We set H to 200 dbar for Cases 2 and 4 (Figs. 7 and 9) to exclude the effects of changes in the main thermocline. During Cases 2 and 4 (Fig. 12), when the two floats observed a similar water mass, we suggested that stratification in the ML was caused by geostrophic adjustment and/or ML eddy formation related to wintertime cooling and smaller Ekman transports after the storms. We speculate that the formation of ML eddies was important for Case 4 because the intervals between storms were longer in late winter and the satellite data (Fig. 10) showed submesoscale cyclonic eddies at that time.

5. Conclusions

This paper focuses on four post-storm restratification events that were observed by two autonomous BGC floats during February to April 2018 in the subtropical northwestern Pacific.

https://doi.org/10.5194/os-2021-38
Preprint. Discussion started: 25 May 2021

The BGC data acquired were stoichiometrically analyzed by Sukigara et al. (2021; this issue).

From February to April, periods of strong wind became shorter and calm intervals between storms increased. To exclude the effects of water advection and float movement, we calculated temporal changes of heat content and the one-dimensional heat budget. During the events when the two floats observed relatively uniform water in the ML, daily average surface heat fluxes we calculated were indicative of cooling during January to March and suggest that ML restratification was driven by geostrophic adjustment or the formation of ML eddies.

At the end of March, high surface concentrations of chlorophyll *a* were observed within submesoscale eddies and at the edge of a mesoscale cyclonic feature identified from satellite data. From the ***Q***-vector distribution and PV balance, we speculate that upwellings caused by an enhanced mesoscale cyclonic feature in late March caused local increases of nutrient concentrations below the ML. Then, nutrients were entrained in the deepening ML during sporadic storms and restratification related to the formation of eddies in the ML led to high surface concentrations of chlorophyll *a*. Therefore, we conclude that primary production in the subtropical northwestern Pacific was enhanced by the combined effects of mesoscale upwelling, formation of a deep ML due to storm activity, subsequent formation of ML eddies, weak daily average cooling (increasing sunlight), and longer intervals between storms.

https://doi.org/10.5194/os-2021-38
Preprint. Discussion started: 25 May 2021

Acknowledgements

We are indebted to the captain and crew of R/V Shinsei Maru for their seamanship. We thank H. Hosoda, M. Hirano and K. Sato at JAMSTEC and T. Iino at Marine Works Japan Ltd. (MWJ) for their helps for operation and calibration of BGC Argo floats, and K. Katayama, S. Oshitani, and H. Tamada at MWJ for their onboard analysis and deck work. We thank A. Fassbender at NOAA Pacific Marine Environment Laboratory and Y. Takeshita at Monterey Bay Aquarium Research Institute for their onboard analysis and discussions. We also thank D. Hasegawa and T. Okunishi at Tohoku National Fisheries Research Institute for operating the SeaGlider. This experiment was supported by Grant in Aid for Scientific Research on Innovative Areas (Ministry of Education, Culture, Sports, Science and Technology [MEXT] KAKENHI JP15H05818 and JP15K21710). The SeaGlider survey was partly supported by Japan Society of Promotion of Science through Grants-in-Aid for Scientific Research in Innovative Areas 2205. TN was supported by Grant in Aid for Scientific Research (MEXT KAKENHI 16H01590, 18H04914, 19H01965 and 20K20634).

References

https://doi.org/10.5194/os-2021-38
Preprint. Discussion started: 25 May 2021

Cronin, M. F., Bond, N. A., Farrar, J. T., Ichikawa, H., Jayne, S. R., Kawai, Y., Konda, M., Qiu, B., Rainville, L., and Tomita, H.: Formation and erosion of the seasonal thermocline in the Kuroshio Extension recirculation gyre, Deep Sea Res., Part II, 85, 62–74, doi:10.1016/j.dsr2.2012.07.018, 2013.

Ducet, N., Le Traon, P. Y., and Reverdin, G.: Global high-resolution mapping of ocean circulation from the combination of T/P and ERS-1/2, J. Geophys. Res., 105, 19477-19498, 2000.

Fassbender, A. J., Sabine, C. L., Cronin, M. F., and Sutton, A. J.: Mixed-layer carbon cycling at the Kuroshio Extension Observatory, Global Biogeochem. Cycles, 31, 272– 288, doi:10.1002/2016GB005547, 2017.

Fox-Kemper, B., Ferrari, R., and Hallberg, R.: Parameterization of Mixed Layer Eddies. Part I: Theory and Diagnosis, J. of Phys. Oceanogr., 38(6), 1145-1165, 2008.

Hoskins, B. J., Draghici, I., Davies, H. C.: A new look at the ω-equation, Quart. J. R. Met. Soc., 104, 31–38, 1978.

Mahadevan, A.: The Impact of Submesoscale Physics on Primary Productivity of Plankton, Ann Rev Mar Sci. 2016 8:1, 161-184, 2016.

https://doi.org/10.5194/os-2021-38
Preprint. Discussion started: 25 May 2021

Mahadevan, A., D'Asaro, E., Lee, C., Perry, MJ.: Eddy-driven stratification initiates North Atlantic spring phytoplankton blooms, Science, Jul 6;337(6090):54-8. doi: 10.1126/science.1218740. PMID: 22767922, 2012.

McGillicuddy, D. J., Robinson, A. R., Siegel, D. A., Jannasch, H. W., Johnson, R., Dickey, T. D., McNeil, J., Michaels, A. F., and Knap, A. H.: Influence of mesoscale eddies on new production in the Sargasso Sea, Nature, 394, 263–266, 1998.

Oka, E., Ishii, M., Nakano, T., Suga, T., Kouketsu, S., Miyamoto, M., Nakano, H., Qiu, B., Sugimoto, S., and Takatani, Y.: Fifty years of the 137E repeat hydrographic section in the western North Pacific Ocean, J. Oceanogr., 74, 115-145, 2018

Oka, E., Yamada, K., Sasano, D., Enyo, K., Nakano, T., and Ishii, M.: Remotely forced decadal physical and biogeochemical variability of North Pacific Subtropical Mode Water over the last 40 years, Geophys. Res. Letters, 46, 1555-1561, 2019

Redfield, A. C.: The Biological Control of Chemical Factors in the Environment, American Scientist, 46, 3, 205–21, 1958

Riser, S. and Johnson, K.: Net production of oxygen in the subtropical ocean, Nature, 451, 323–325, https://doi.org/10.1038/nature06441, 2008

Stone, P. (1970). On non-geostrophic baroclinic stability: Part II. J. Atmos. Sci., 27, 721–726.

Wenegrat, J.O., L. N. Thomas, J. Gula, and J. C. McWilliams (2018). Effects of the submesoscale on the potential vorticity budget of ocean mode waters. J. Phys. Oceanogr. 48, 9, 2141-2165.

Tandon, A. and C. Garrett (1995). Geostrophic Adjustment and Restratification of a Mixed Layer with Horizontal Gradients above a Stratified Layer, Journal of Physical Oceanography, 25(10), 2229-2241. doi: 10.1175/JPO-D-17-0219.1.

Taylor, J. and R. Ferrari (2009). The role of secondary shear instabilities in the equilibration of symmetric instability. J. Fluid Mech., 622, 103–113, doi:10.1017/S0022112008005272.

Taylor, J. and R. Ferrari (2010). Buoyancy and wind-driven convection at mixed-layer density fronts. J. Phys. Oceanogr., 40, 1222–1242, doi:10.1175/2010JPO4365.1.

Thomas, L. N. (2005). Destruction of potential vorticity by winds. J. Phys. Oceanogr., 35, 2457–2466, doi:10.1175/JPO2830.1.

Thomas, L. N. and C. M. Lee (2005). Intensification of Ocean Fronts by Down-Front Winds, J. Phys. Oceanogr., 35, 1086-1102.

Thomas, L. N. and R. Ferrari (2008). Friction, frontogenesis, and the stratification of the surface mixed layer, J. Phys. Oceanogr., 38, 2501-2518.

Wenegrat, J. O., L. N. Thomas, J. Gula, and J. C. McWilliams (2018). Effects of the

https://doi.org/10.5194/os-2021-38
Preprint. Discussion started: 25 May 2021

submesoscale on the potential vorticity budget of ocean mode waters. J. Phys. Oceanogr. 48, 9, 2141-2165.

https://doi.org/10.5194/os-2021-38
Preprint. Discussion started: 25 May 2021

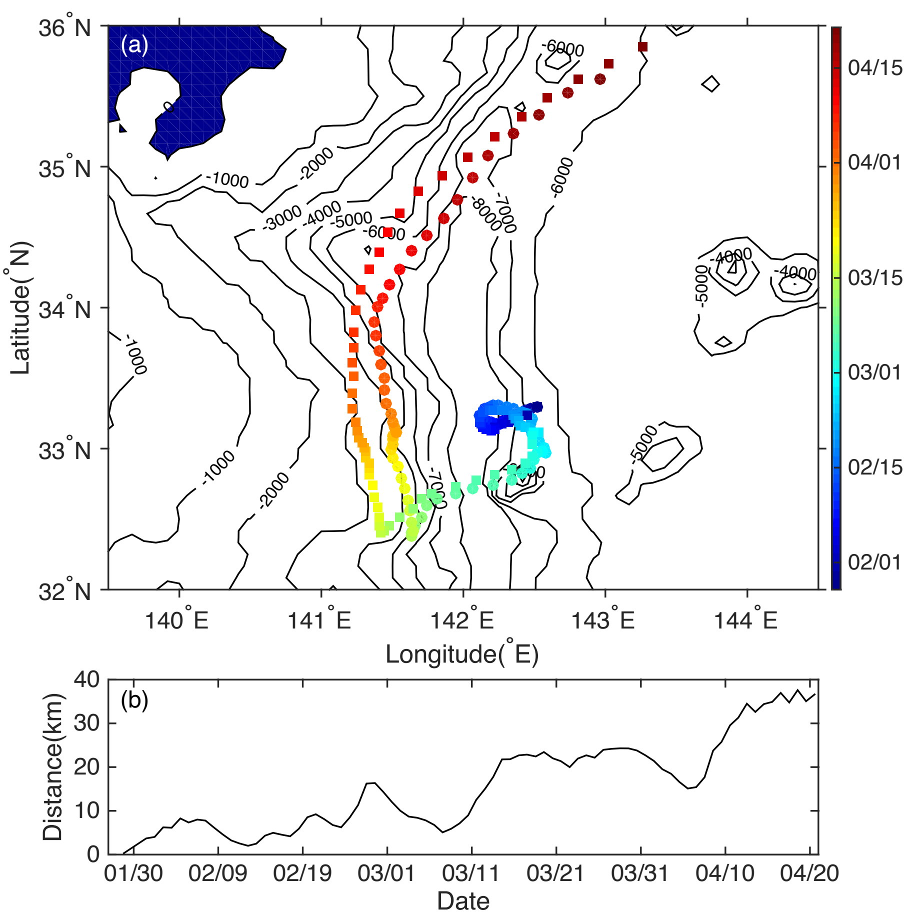

374

375 Figure 1. (a) Trajectories of the two BGC-Argo floats used in this study. Circles and squares
376 indicate the positions of float nos. 2903329 and 2903330, respectively. (b) Temporal changes of
377 the distance between the two floats.

378

https://doi.org/10.5194/os-2021-38
Preprint. Discussion started: 25 May 2021

Ocean Science
Discussions

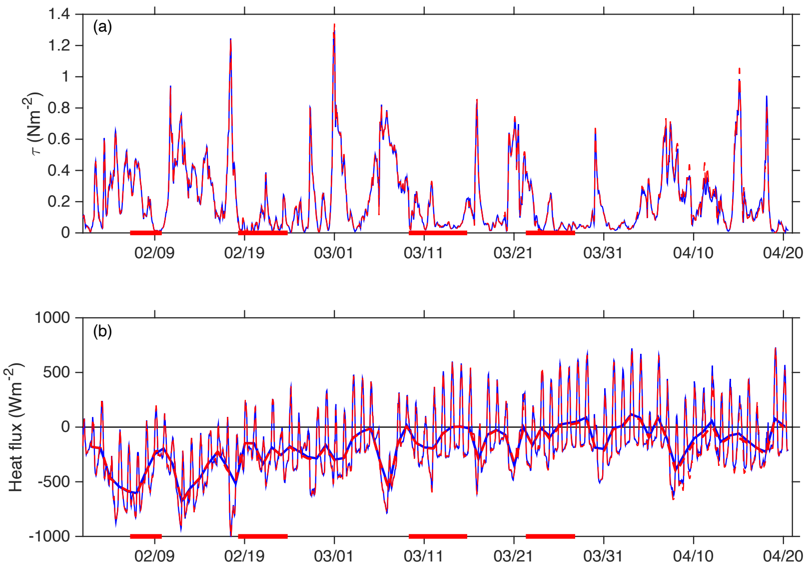

Figure 2. (a) Hourly wind stress and (b) heat flux at float positions. Hourly float positions were linearly interpolated between daily positions. Blue solid and red dashed lines indicate data for float nos. 2903329 and 2903330, respectively. Thick red and blue lines in (b) show 24-h running averages. The thick red lines at the bottom of each plot mark the durations of the post-storm restratification events shown in Table 1. Negative values in panel (b) represent surface cooling.

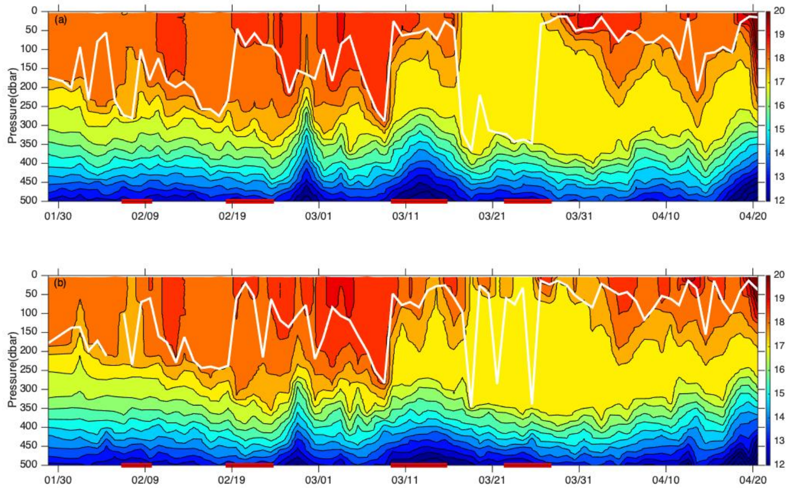

Figure 3. Time series of vertical potential temperature profiles observed by BGC-Argo float nos. (a) 2903329 and (b) 2903330. The white line indicates the depth of the ML. The thick red lines at the bottom of each panel mark the durations of the post-storm restratification events shown in Table 1.

https://doi.org/10.5194/os-2021-38
Preprint. Discussion started: 25 May 2021

Ocean Science
Discussions
Open Access
EGU

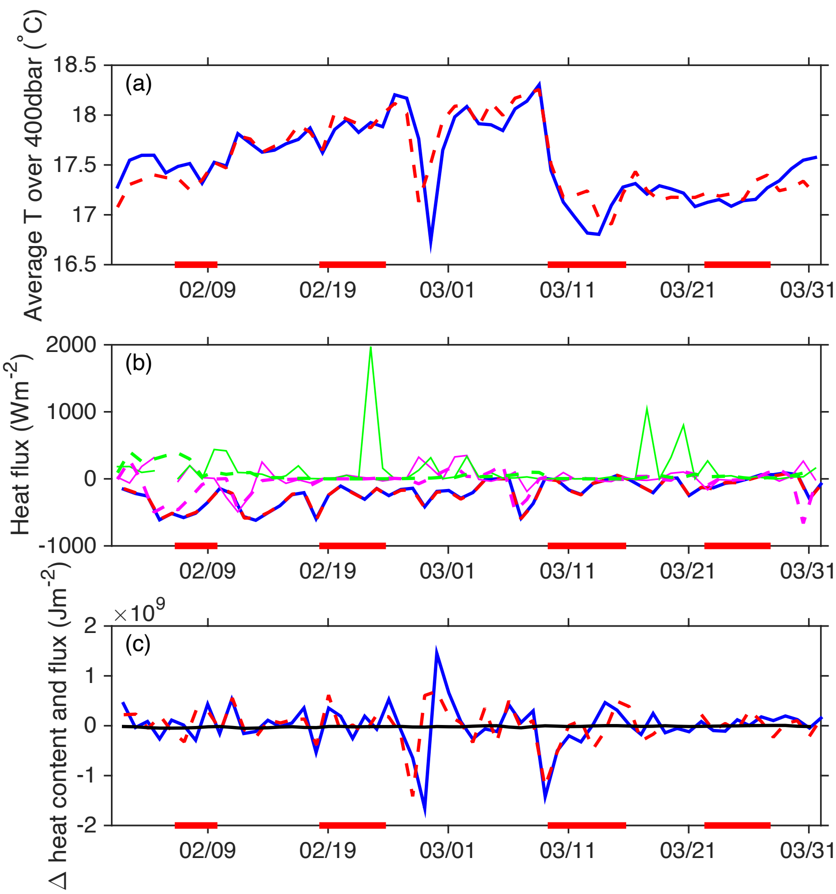

Figure 4. Time series for both floats of (a) average potential temperature above the 400 dbar level (b) surface heat flux, and (c) changes of heat content and cumulative heat flux (thick black line). In all panels, the blue and red dashed lines represent data of float nos. 2903329 and 2903330, respectively. Red thick lines on the bottom of each panel indicate the storm events (Table 1). In panel (b), the green and magenta lines show F_{ME} and F_{EK}, respectively, from float data (thin lines) and the modeled values (thick dashed lines).

https://doi.org/10.5194/os-2021-38
Preprint. Discussion started: 25 May 2021

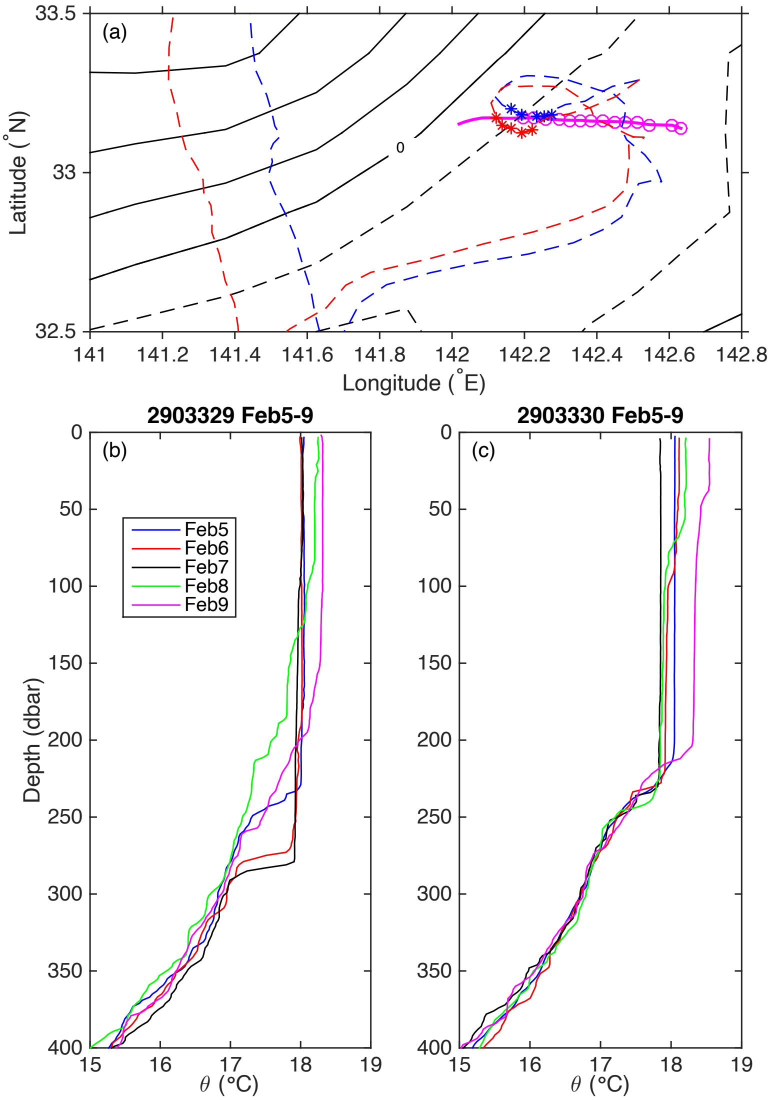

Figure 5. (a) SSHA contours on 7 February and BGC float trajectories (blue and red dashed lines indicate float nos. 2903329 and 2903330, respectively). Solid and dashed lines are positive and negative, respectively. Contour interval is 0.05 m. Blue and red asterisks are daily float positions

https://doi.org/10.5194/os-2021-38
Preprint. Discussion started: 25 May 2021

between 5 and 9 February. The magenta line shows the trajectory of the SeaGlider between 7 and 10 February, and the magenta circles are observation positions between 7 and 9 February. (b) and (c) Vertical profiles from 5 to 9 February of potential temperature from float nos. 2903329 and 2903330.

https://doi.org/10.5194/os-2021-38
Preprint. Discussion started: 25 May 2021

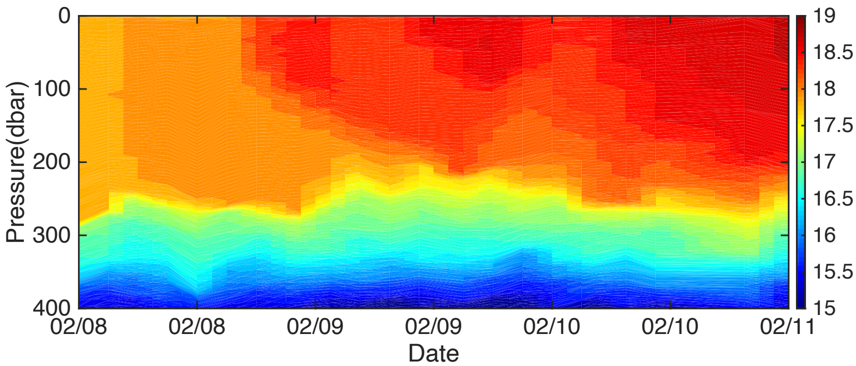

Figure 6. Time series of the vertical profile of potential temperature from SeaGlider data. The fixed time (at the start of profiling) is used for generating the figure.

https://doi.org/10.5194/os-2021-38
Preprint. Discussion started: 25 May 2021

Ocean Science
Discussions
Open Access

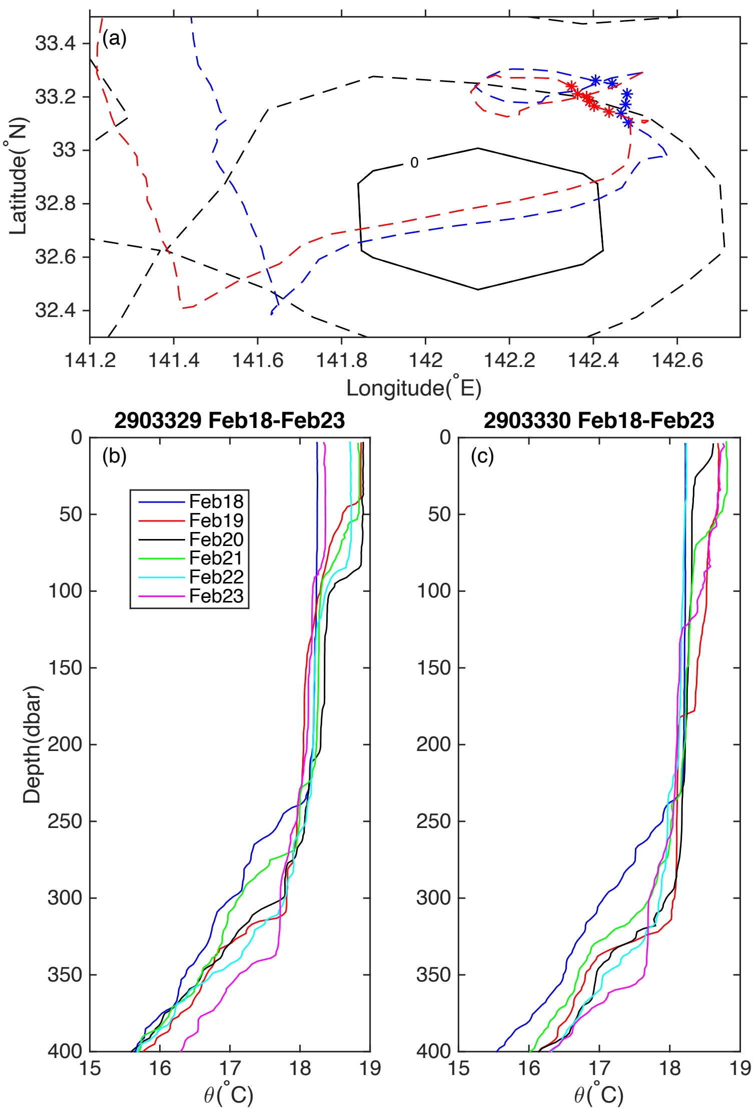

418

419 Figure 7. Same as Figure 5 but for Case 2. SSHA contours in (a) are for 20 February. Asterisks in

420 (a) are BGC float profiling positions between 18 and 23 February. Vertical profiles in (c) and (d)

421 are for 18 to 23 February.

https://doi.org/10.5194/os-2021-38
Preprint. Discussion started: 25 May 2021

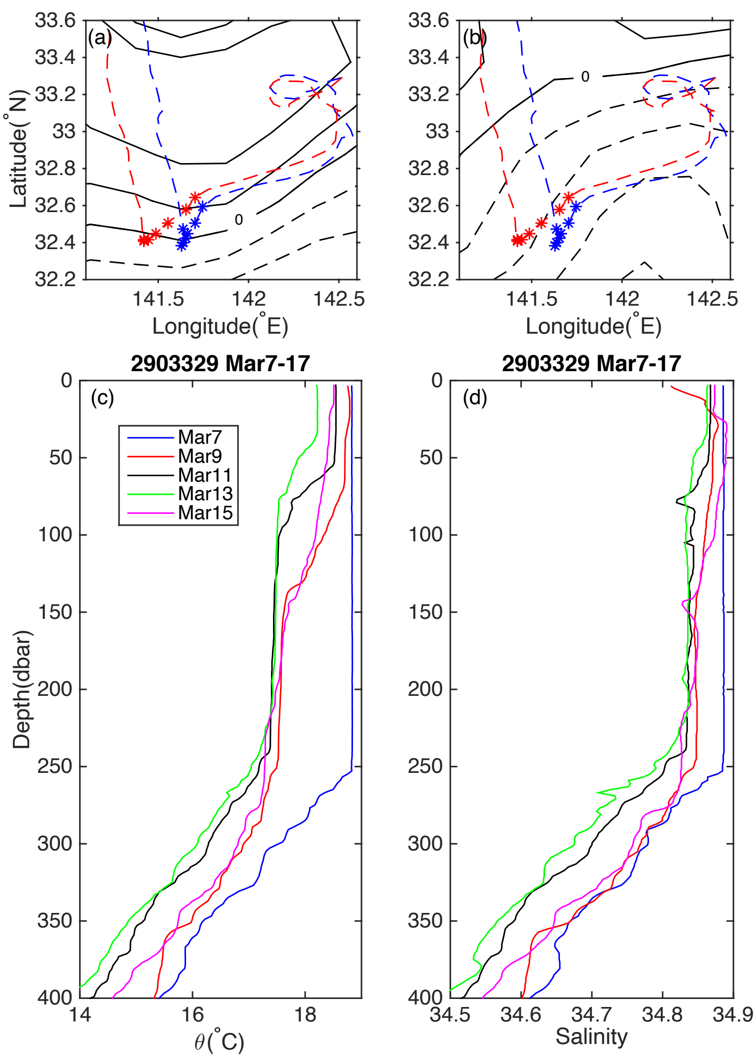

422

423 Figure 8. Same as Figure 5 but for Case 3. (a) and (b) SSHA contours for 8 and 13 March,
424 respectively. (c) and (d) Vertical profiles on alternate days from 7 to 15 March of potential
425 temperature and salinity, respectively, from BGC float no. 2903329.

https://doi.org/10.5194/os-2021-38
Preprint. Discussion started: 25 May 2021

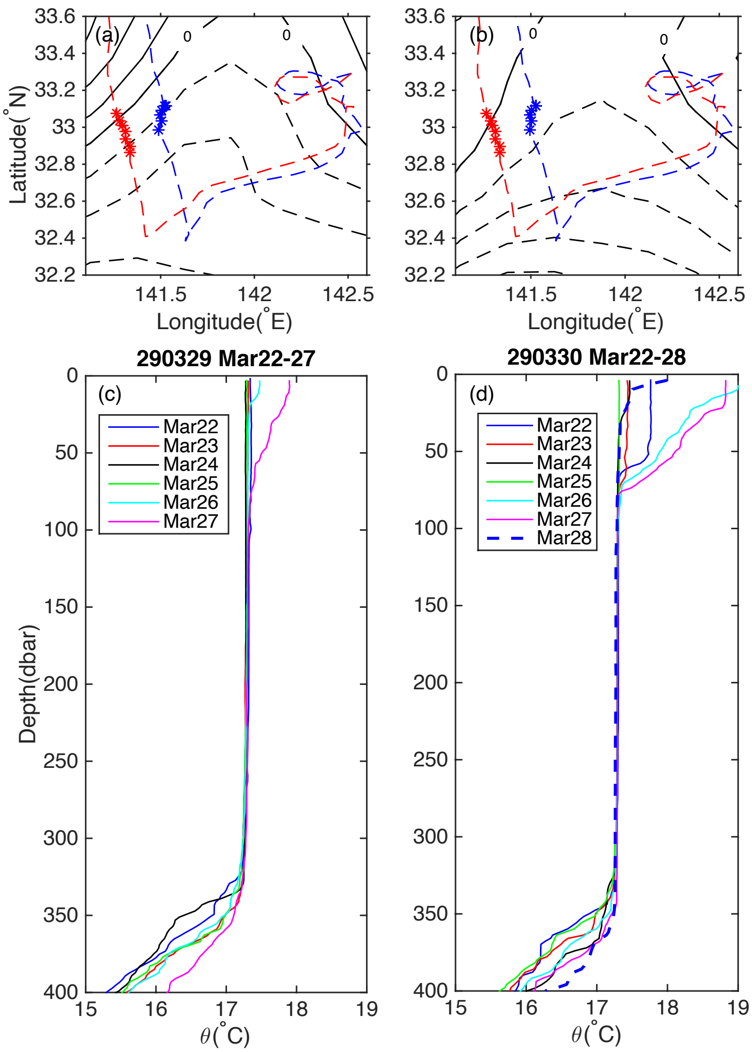

426

427 Figure 9. Same as Figure 5 but for Case 4. (a) and (b) SSHA contours for 22 and 27 March,

428 respectively. (c) and (d) Vertical profiles from 22 to 27 March of potential temperature from BGC

429 float nos. 2903329 and 290330.

https://doi.org/10.5194/os-2021-38
Preprint. Discussion started: 25 May 2021

Ocean Science
Discussions

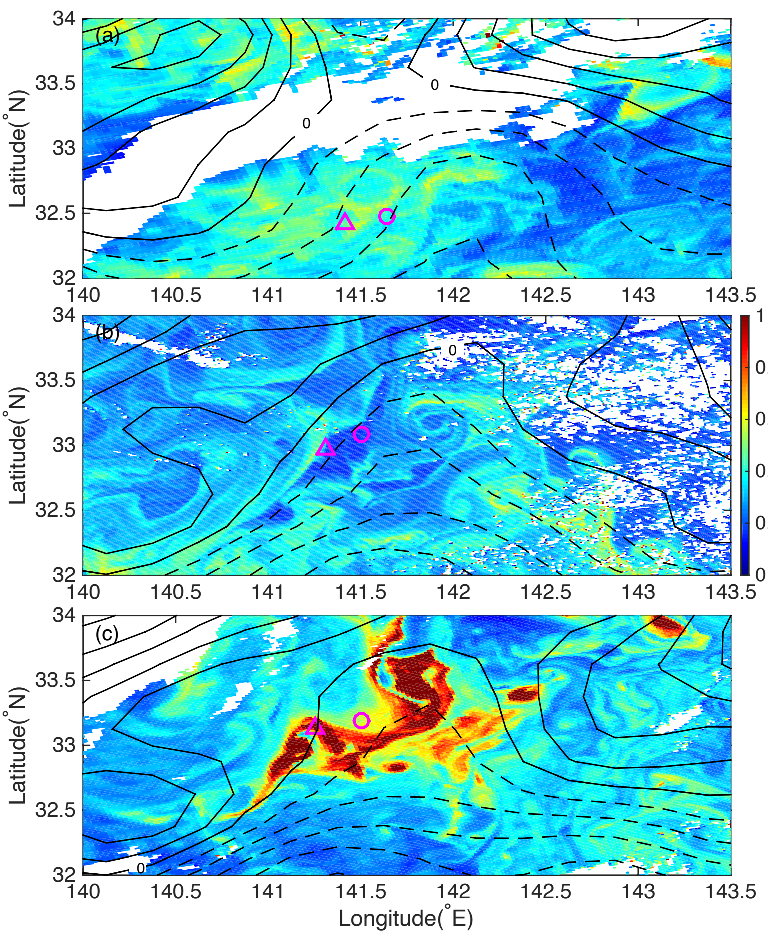

Figure 10. SSHA contours and sea surface chlorophyll *a* concentrations (mg m^{-3}, color scale) derived from satellite data on (a) 15 March, (b) 25 March, and (c) 29 March. Solid and dashed lines are positive and negative, respectively. Contour interval is 0.05 m. The magenta circles and triangles show the positions of BGC float nos. 2903329 and 2903330, respectively. Storms (see Table 1 and Fig. 2) passed through this area on 7 March (before Case 3) and 21 March (before Case 4).

https://doi.org/10.5194/os-2021-38
Preprint. Discussion started: 25 May 2021

Ocean Science
Discussions
Open Access

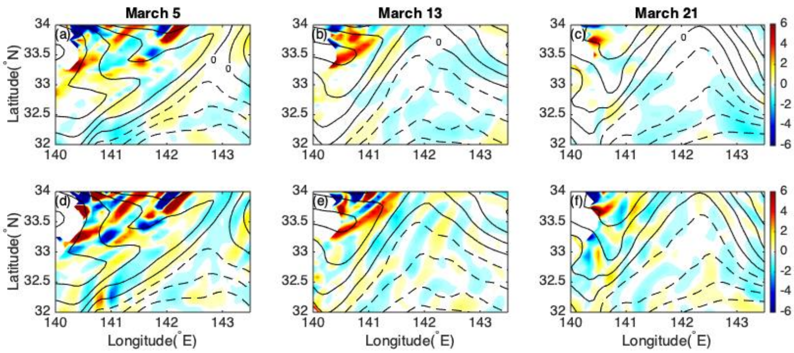

Figure 11. Horizontal distributions of (a–c) the normalized $\boldsymbol{Q}$ vector, $10^{13} \times Q \cdot \nabla_h b / |\nabla_h b|$, and (d–f) the horizontal divergence of the $\boldsymbol{Q}$ vector, $10^{17} \times -\nabla_h \cdot Q$, at 380 m. (a) and (d) are for 5 March, (b) and (e) for 13 March, and (c) and (f) for 21 March. Contours show modeled SSHA (difference between SSH and the time-averaged SSH for January–March). Solid and dashed contours represent positive and negative values, respectively. The contour interval is 0.05 m.

https://doi.org/10.5194/os-2021-38
Preprint. Discussion started: 25 May 2021

Ocean Science
Discussions
Open Access
EGU

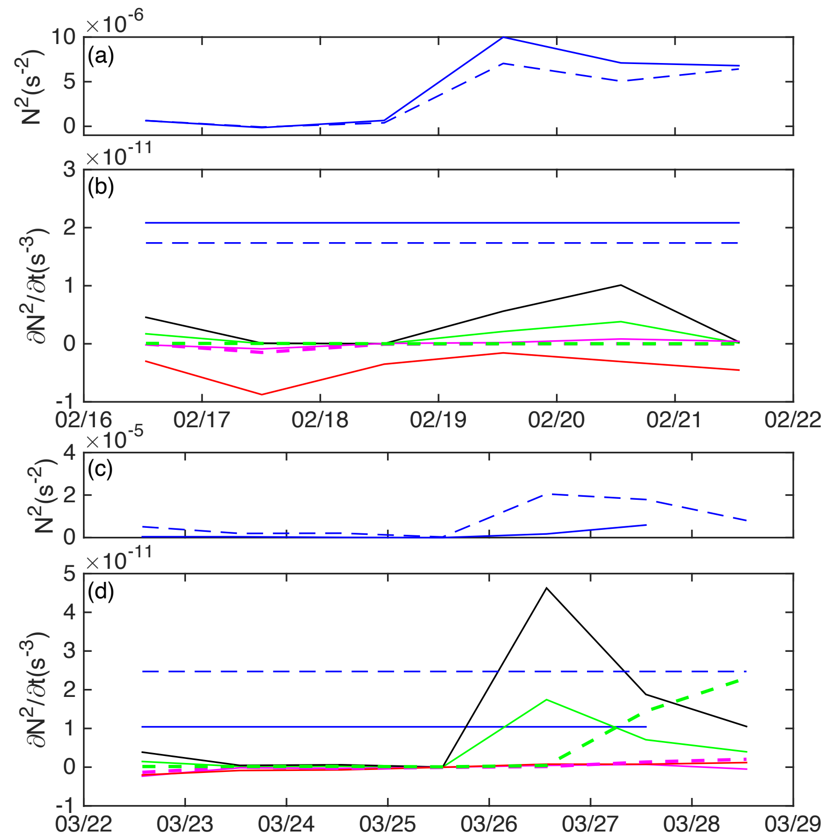

Figure 12. Time series of (a) and (c) buoyancy frequency squared, N^2, and (b) and (d) rate of change of buoyancy frequency squared, $\partial N^2/\partial t$. Solid and dashed blue lines are for BGC float nos. 2903329 and 2903330, respectively. In (b) and (d), the blue lines were obtained by the linear fit to N^2 in (a) and (c). The solid red lines in (b) and (d) are $\partial N^2_{BUO}/\partial t$; the solid black lines are $\partial N^2_{GEO}/\partial t$ from float data; the green solid and dashed lines are $\partial N^2_{ME}/\partial t$ from the BGC float data and the model, respectively; and the magenta solid and dashed lines are $\partial N^2_{EK}/\partial t$ from the BGC float data and the model, respectively.

https://doi.org/10.5194/os-2021-38
Preprint. Discussion started: 25 May 2021

Table 1. Stoichiometric comparison of the surface layer in each post-storm restratification events (case 1-4) adapted from Sukigara et al. (2021)

Table 1.

Float #	Event period Start – End (days)	POC increment [µmolC kg^{-1} d^{-1}]	NO_3^- decrement [µmolN kg^{-1} d^{-1}]	CN ratio
Case 1 (Storm on 5th Feb.)				
2903329	6th -9th Feb. (3 days)	0.402	-0.264	-1.5
2903330	6th -9th Feb. (3 days)	0.148	-0.213	0.7
Case 2 (Storm on 17th Feb.)				
2903329	18th -23rd Feb. (5 days)	0.184	-0.028	-6.7
2903330	18th -23rd Feb. (5 days)	0.298	-0.057	-5.2
Case 3 (Storm on 7th Mar.)				
2903329	9th -15th Mar. (6 days)	0.310	-0.039	-8.1
2903330	9th -15th Mar. (6 days)	0.148	0.012	+12.7
Case 4 (Storm on 21st Mar.)				
2903329	22nd -27th Mar. (5 days)	0.785	-0.181	-4.3
2903330	22nd -28th Mar. (6 days)	0.613	-0.078	-7.8